

# Performance of G-Oil Well cement exposed to elevated hydrothermal curing conditions

Martin T. Palou · František Šoukal ·  
Martin Boháč · Pavel Šiler · Tomáš Ifka ·  
Vladimír Živica

Received: 31 October 2013 / Accepted: 4 June 2014 / Published online: 8 July 2014  
© Akadémiai Kiadó, Budapest, Hungary 2014

**Abstract** G-Oil Well cement was modified by blending it with blast furnace slag and silica fume at various ratios. The hydration was carried out under the hydrothermal conditions (200 °C and 1.2 MPa) up to 7 days. TG and DTG were performed on cured pastes to identify the hydrated products, their quantity and their stability under given hydrothermal curing conditions. The microstructure of samples was observed by a scanning electron microscope. The mechanical compressive strength was determined and the pore structure was analyzed using mercury intrusion porosimeter. It was found out that the compressive strength values of blend G-Oil Well cements markedly increased with increasing blast furnace/silica ratio. The pore structure was consolidated, as demonstrated by the displacement of pore size distribution to the region of micro and nano pores.

**Keywords** G-Oil Well cement · Hydrothermal curing · Thermal analysis · Hydrate products · Compressive strength · Porosity · Microstructure

## List of symbols

C CaO  
A Al<sub>2</sub>O<sub>3</sub>  
F Fe<sub>2</sub>O<sub>3</sub>  
S SiO<sub>2</sub>  
H H<sub>2</sub>O

## Introduction

The hydration reactions that run during cementing petroleum, gas, and geothermal wells are strongly influenced by the temperature and steam pressure of fluid surrounding the steel casing [1–5] like those occurring under “hydrothermal curing regimes” [6–10]. In these conditions, temperatures and pressures are so high that they challenge the durability of construction materials placed in the annular space between the well steel casing and the geological formations surrounding the well bore to provide zonal isolation. In addition to the effect of high pressure and temperature, the oil well cement slurries must be able to contend with weak or porous structures because of the permeability to corrosive fluids. A successful oil well cementing must have low permeability and adequate durability to ensure the long-term isolation of the producing formation [2]. For cementing these wells as protective layer during the exploitation of natural gas and petroleum, the API (American Petroleum Institute) Specifications for Materials and Testing for Well Cements (API Specification 10A, 2002) has established 9 Special classes of cements (Class A–Class J), of which Class G and Class H are widely used in well cementing [11]. They are arranged according to the depths, to which they are placed, and the pressures and temperatures to which they are exposed. G-Oil Well cements are usually made from Portland cement clinker or from blended hydraulic cements. The most dominant minerals are essentially tricalcium silicate (C<sub>3</sub>S, 3CaO·SiO<sub>2</sub>) and dicalcium silicate (C<sub>2</sub>S, CaO·SiO<sub>2</sub>) supplemented by tetracalcium aluminoferrite (C<sub>4</sub>AF, 3CaO·Al<sub>2</sub>O<sub>3</sub>·Fe<sub>2</sub>O<sub>3</sub>), but with lower amount of tricalcium aluminate (C<sub>3</sub>A, 3CaO·Al<sub>2</sub>O<sub>3</sub>) in order to avoid sulfate attack. It is recommended to use G-Oil Well cement up to 120 °C. In our recent studies [2], it was proved that the

M. T. Palou · F. Šoukal · M. Boháč · P. Šiler  
Faculty of Chemistry, Brno University of Technology,  
Purkyňova 118, 612 00 Brno, Czech Republic

M. T. Palou (✉) · T. Ifka · V. Živica  
Institute of Construction and Architecture, Slovak Academy of  
Sciences, Dúbravská 9, 845 03 Bratislava 45, Slovak Republic  
e-mail: martin.palou@stuba.sk

hydration of G-Oil well cement at normal conditions leads to the formation of a gelatinous calcium silicate hydrates (C–S–H) that are responsible for necessary strength and dimensional stability of set cement. Also, an important amount of calcium hydroxide and calcium carbonate is formed during the curing process. When cured under different hydrothermal conditions with increasing temperature and steam pressure (0.3 MPa/120 °C, 1.2 MPa/150 °C, 2.0 MPa/200 °C), C–S–H gel is transformed into  $\alpha$ -C<sub>2</sub>SH at 150 °C and then into C<sub>6</sub>S<sub>2</sub>H<sub>3</sub> at 200 °C. This transformation of C–S–H to  $\alpha$ -C<sub>2</sub>SH and C<sub>6</sub>S<sub>2</sub>H<sub>3</sub> under autoclave curing has caused the depletion of microstructure, the degradation of pore structure and the decrease in compressive strength known as strength retrogression. Consequently, G-Oil well cement is not suitable for cementing well at temperature more than 150 °C. Authors [3–5, 12] have reported the similar behavior of Ordinary Portland cement cured under different saturated steam pressure and temperatures. Between 120 and 350 °C, moderately permeable xonotlite (Ca<sub>6</sub>Si<sub>6</sub>O<sub>17</sub>(OH)<sub>2</sub>) associated with volume reduction appeared as a major product [4] causing a relative decrease of compressive strength. Therefore, several attempts have been undertaken to avoid this strength loss by the use of products which could stabilize tobermorite, in which the ratio C/S is nearly equal to 1 [5, 10]. In other words, the occurrence of  $\alpha$ -C<sub>2</sub>SH at temperature over 120 °C can be prevented by reducing lime-to-silica ratio (C/S ratio) in the cement [5, 8]. C–H–S gel has a variable C/S ratio, averaging about 1.5 [12]. For this purpose, silica-rich additives such as fly ash, silica flour or silica fume were added to the Portland cement to lower C/S ratio to about 1.0. As the application of silica fume inhibits the hydration of C<sub>3</sub>S and not only crystallization of CSH, the synergic effect of the pressure and temperature in the autoclave on the acceleration of hydration of the cement-microsilica blends has been reported [13, 14]. Midgley and Chopra [10] studied the lime-rich part in the system CaO–SiO<sub>2</sub>–H<sub>2</sub>O in autoclave at 150 °C for 30 days. Using thermal analysis method, they claimed that the presence of  $\alpha$ -C<sub>2</sub>SH was demonstrated by endothermic peak at 460 °C.

Palou et al. [15] have investigated the effect of hydrothermal curing on the hydration of blend Ordinary Portland cement, High Alumina Cements, and Poly-Sodium phosphate fiber-reinforced. Two kinds of hydration products were formed under hydrothermal conditions. The first ones consisted of ordinary hydration products like C–S–H, C–S–A–H, C–A–H, and calcium carbonate as a product of carbonation. The second ones were the products chemically bound like in ceramics as hydroxyapatite and gibbsite.

There are a relatively smaller number of papers describing the structure and performance of G-Oil Well cement blends due to the coupled effect of BFS and SF. Therefore, the present study was undertaken to upgrade the

performances of G-Oil well cement under higher hydrothermal temperature and pressure by adding blast furnace slag (BFS) and silica fume (SF) at different ratios. For this propose, laboratory autoclave was used to simulate hydrothermal regimes similar to those found in geothermal wells, where temperature may exceed 150 °C.

## Experimental

Samples were cured at hydrothermal condition of 1.2 MPa (200 °C) with autoclaving duration of 7 days in laboratory autoclave (High Pressure Autoclave Testing Bluhm & Feuerherdt GmbH). The hydration products formed under hydrothermal conditions and their stability were investigated by simultaneous thermal analysis (DTG and TG) Mettler Toledo TGA/DSC STRA system (Mettler-Toledo, Switzerland). After compressive strength test, a part of sample was dried in an electric oven at 105 °C to remove water physically bound before it was milled. Approx. 50 mg of sample was placed in an open vessel under air atmosphere, and measured at a heating rate of 10 °C min<sup>-1</sup> up to 1000 °C. The compressive strength was tested using compressive testing machines WPN VEB Thüringer Industrierwerk Rauenstein 11/2612 (25 000 N). Mercury intrusion porosimeter Quantachrome Poremaster 60GT (Quantachrome UK Limited) was used for the determination of pore structure characteristics, pore size distribution, and permeability. Mercury intrusion porosimetry provides a curve of pore size distribution (PSD) versus pore size. Two or three pieces of the dried sample with diameter less than 10 mm and total mass max. 2 g were used for the tests. The maximum applied pressure of mercury was 414 MPa, equivalent to a Washburn pore radius of 1.8 nm. Scanning Electron Microscope, SEM TESLA BS 300) was used for microstructure observations. The samples were sputtered coated with Au before observation.

Oil well Portland cement without mineral components denoted as Class G HSR was from Holcim OJSC “Volskement,” Saratov region, Russia. The chemical composition of cement and mineralogical composition of clinker given by the producer are reported in Table 1.

Five cement mixtures denoted (GOWC0–GOWC5) were prepared by blending GOWC with blast slag furnace (BFS) and silica fume (SF) and cured under hydrothermal conditions of 1.2 MPa and 200 °C. The composition is reported in Table 2.

### Mixing procedure, autoclaving, and test specimens

Pastes were prepared by mixing different blended Oil well cements with an adequate quantity of water as determined by workability procedure (water to cement ratio depends on BFS/SF ratio in mixtures). Six prisms with the

**Table 1** Oxide and mineralogical composition of used materials

Oxide	Oxide composition/%			Mineral composition of GOWC		
	GOWC	BFS	SF	Designation	Formula	Composition
CaO	64.0	36.53	0.50	Alite	3CaO·SiO <sub>2</sub>	65.0
SiO <sub>2</sub>	21.0	35.76	97.10	Belite	2CaO·SiO <sub>2</sub>	12.0
Al <sub>2</sub> O <sub>3</sub>	4.5	9.39	0.21	Aluminates	3CaO·Al <sub>2</sub> O <sub>3</sub>	2.5
Fe <sub>2</sub> O <sub>3</sub>	5.5	0.24	–	Aluminate-ferrites	4CaO·Al <sub>2</sub> O <sub>3</sub> ·Fe <sub>2</sub> O <sub>3</sub>	17.5
MgO	1.5	14	0.40			
SO <sub>3</sub>	2.5	0.03				
Spec. surface/cm <sup>2</sup> g <sup>-1</sup>	3300	4700	15000			
	Blaine	Blaine	(BET)			

**Table 2** Composition of blended G-Oil Well cements/%

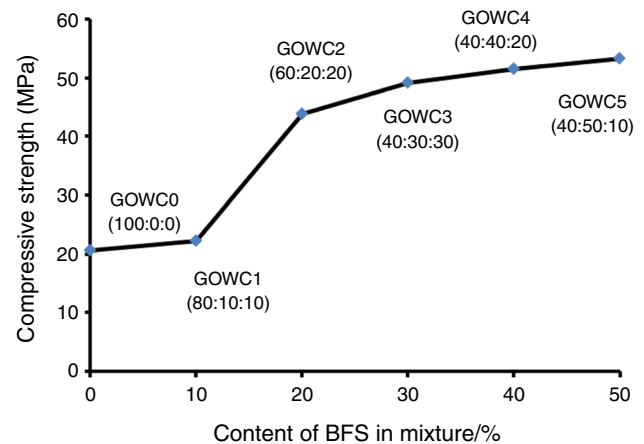
Blended cement	GOWC	BFS	SF	SF/GOWC
GOWC0	100	0	0	–
GOWC1	80	10	10	0.125
GOWC2	60	20	20	0.33
GOWC3	40	30	30	0.75
GOWC4	40	40	20	0.5
GOWC5	40	50	10	0.25

dimensions of 160 × 40 × 40 mm were prepared from paste to be cured under at hydrothermal condition of 1.2 MPa/200 °C during 7 days. Molds filled with fresh paste were then embedded into drying chamber. The specimens were exposed to steam curing condition at 100 °C for 30 min and after this precuring procedure still hot hardened specimens were quickly demolded and inserted into the autoclave. At the 7th day of autoclaving, the hot prisms were taken off and inserted in hot water. Cooling of water was accelerated gradually by adding of cold water as the handling temperature of approximately 40 °C was achieved. The compressive was tested on three samples; the average values of the compressive strength of samples were calculated and recorded as the total compressive strength.

## Results and discussion

### Compressive strength

The first performance of blended GOWC cured under 1.2 MPa/200 °C is demonstrated by the values of compressive strength that has been found depending on the OPC/(BFS + SF) ratio in the mixtures (Fig. 1). The compressive strength of G-Oil Well cement without addition is 20.60 ± 4 MPa. The value increases with the addition of BFS and SF. The depletion of compressive due to

**Fig. 1** Influence of BFS and SF addition on the performance of compressive strength

increasing hydrothermal temperature and pressure, as reported in [2], has been stopped and upgraded with the presence of mineral admixtures. This performance results from the presence of more stable hydrated products formed by pozzolanic reaction of SF and BFS.

### Thermal analysis of cured samples

In order to understand the hydration reaction that led to the formation of stable hydrated products and their influence on the compressive strength of autoclaved blended GOWC, DTG, and TG curves was deeply analyzed. Figures 2 and 3 depict the overall DTG and TG curves of all samples between 0 and 1000 °C. As the velocity of thermal decomposition of Ca(OH)<sub>2</sub> is too high in GOWC0 and reduces the endothermic peaks of other process, different main interval temperatures were considered to explain the effect of BFS and SF addition on the hydration of GOWC. It is evident that such temperature intervals 0–280, 280–480, 480–600, and 600–1000 °C with significant

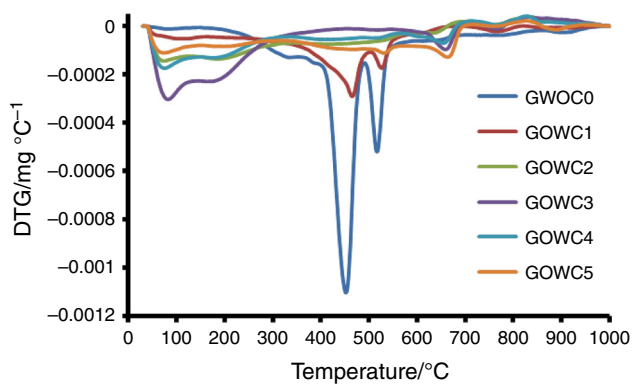


**Fig. 2** Influence of BFS and SF content on DTG characteristics of autoclaved samples

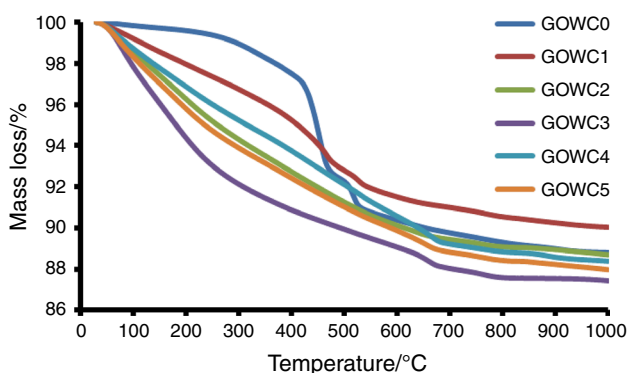


**Fig. 3** Influence of BFS and SF at constant ration on TG characteristics of autoclaved samples

endothermic peaks can be investigated with regard to the evolution of hydrated products influenced by the coupled effect of temperature and pressure in autoclave. The TG curves plotted in Fig. 3 quantify the mass loss (%) due to the decomposition of hydrated and carbonated products. From TG curves, relative mass loss (%) in different temperature intervals was calculated from the overall mass loss

of thermally decomposed products. The results reported in Table 3 allow to evaluate the preponderance of different products of reaction (hydration and carbonation) for different samples cured under hydrothermal conditions. Despite the fact that DTG curves do not show endothermic or exothermic peaks in some temperature intervals, TG ones (relative mass loss) reveal the existence of some products within them though in negligible quantity.

A specific exothermic peak due to the crystallization in temperature range 800–900 °C from DSC “equivalent” curve from TG/DSC measurement was evaluated also.

TG and DTG curves of GOWC0 have been extensively discussed in our work [2], as the result of the influence of increasing hydrothermal temperature/pressure upon the stability and transformation of CSH to  $C_6S_2H_3$  via  $\alpha$ - $C_2SH$ . This transformation is elucidated by the presence of very weak endothermic peak in the temperature range 0–280 °C, but by the presence of endotherm velocity at 500–560 temperature intervals. To avoid this transformation that led to the strength retrogression and to permeability increase, BFS and SF were added. The effect of this addition is reflected by TG and DTG curves (Figs. 2, 3) with different rates of mass loss in different temperature intervals.

The first important temperature interval 0–280 °C showing two endothermic peaks denotes the thermal decomposition of calcium silicate hydrates (C–S–H) and calcium silicate aluminate hydrates (C–A–S–H) products (Fig. 4). Comparatively with G-Oil Well cement without addition, two endothermic peaks are located at 0–200 °C. The magnitude of the second one is linked with increasing content of BFS in the mixture, while SF is responsible for the first peak and plays an essential role in the diminishment of CH content. It results that the mass loss and the velocity of endothermic peaks depends on the content of mineral additives to GOWC. The lower temperatures of decomposition of C–S–H are probable due to the distortion of tobermorite structure by drying at 105 °C in electric oven.

**Table 3** Relative mass loss (%) of different products in different temperature intervals

Sample	GOWC0	GOWC1	GOWC2	GOWC3	GOWC4	GOWC5
Total mass loss/%	11.19	9.96	11.31	12.57	12	12.03
	Relative mass loss (%)					
Temperature intervals products						
0–280 °C (CSH, CSAH)	7.5	30.12	47.30	59.98	33.33	48.13
400–480 °C (CH)	43.78	21.18	10.61	6.04	11.33	9.47
480–560 °C ( $C_6S_2H_3$ )	17.15	13.15	9.10	5.64	8.33	8.23
600–700 °C (Carbonated1)	5.54	1.00	8.27	8.27	16.66	8.72
700–800 °C (Carbonated2)	4.11	4.51	3.89	3.58	0	3.32
800–1000 °C (Carbonated3)	4.37	5.12	2.74	1.19	7.95	3.74

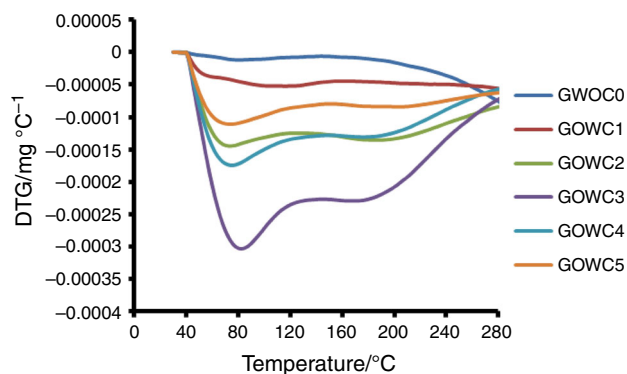


**Fig. 4** Influence of BFS and SF content on DTG characteristics of autoclaved samples in temperature interval 0–280 °C

By exploring the TG curves (Fig. 3) of different cured samples, it is evident that the relative mass loss increases in temperature range 0–200 °C from 7.5 % for GOWC0 to 59.98 % for GOWC3 with increasing SF in the mixtures. The increase in mass loss is due to the liberation of water chemically bond denotes the increasing amount of C–S–H and its stability under hydrothermal curing conditions. This increase characterizes the formation of additional products such gehlenite hydrate ( $C_2ASH_8$ ) due to the pozzolanic activity of SF and BFS [16]. Furthermore, the addition of silica fume decreases the C/S ratio in C–S–H products. These calcium silicate hydrates (tobermorite-like) are more resistant to the destruction effect of hydrothermal curing [14] and are responsible for strength improvement. As it can be observed in Table 3, C–S–H and C–A–S–H became the dominate hydration products.

Temperature range 400–480 °C is characteristic for the thermal decomposition of calcium hydroxide (CH) [17, 18]. Peak intensity of endotherms decreases with increasing addition of BFS and SF. As it was previously reported [14, 17], endotherm characterizing thermal decomposition CH is overlapped with that of  $\alpha$ - $C_2SH$  at 450–500 °C, then the part of CH and  $\alpha$ - $C_2SH$  can be determined from TG curves as mass loss within this temperature interval. The mass loss decreases with increasing content of BFS and SF (GWOC0–43.78 %, GWOC1–21.18 %, GWOC2–15.61 %, and GWOC3 6.04 %). This is attributed not only to the dilution effect (reduction of OPC in mixtures), but mainly to the consumption of CH by pozzolanic reaction and partial carbonation [19–22]. The pozzolanic reaction of BFS and SF were elsewhere deeply described. The process starts with the hydration of tricalcium silicate ( $C_3S$ ) and dicalcium silicate ( $C_2S$ ) that provides CH needful for the activation of pozzolans. [21, 22]. The kinetics of the pozzolanic reaction and the hydration products formed depend on the pozzolan and the portion of calcium hydroxide generated by hydration of Portland

cement. It is known that nano-silica has an accelerating effect on cement hydration. It is assumed that the surface of these particles act as a nucleation site for C–S–H-seeds which then accelerate the cement hydration [13]

GOWC without BFS and SF cured in autoclave is constituted by an important presence of CH because it could not be consumed by pozzolanic reaction.

The main effect of mineral addition is reflected in the temperature range between 480 and 560 °C, where the velocity of endothermic peak decreased with increasing amount of BFS and SF. As it was earlier reported, the endotherm found at this temperature range characterizes  $C_6S_2H_3$  (Jaffeite) thermal decomposition [2, 5, 13, 14].  $C_6S_2H_3$  (Jaffeite) results from the hydrothermal transformation of C–S–H through  $\alpha$ - $C_2SH$  ( $Ca_2SiO_3(OH)_2$ ). The intensity of this endotherm is more pronounced with GOWC0, while no peak is found in GOWC2–5 DTG curves, and the relative mass loss decreases with increasing BFS and SF (GWOC0–17.15 %, GWOC13.15 %, GWOC2–9.10 %, GWOC3 5.64 %). At the highest content of SF and lowest content of OPC, peak characterizing the presence of  $C_6S_2H_3$  has completely disappeared. At the same time, one observe an increase of two endothermic peaks located at the temperature range of 0–200 °C, denoting thus an increase in CSH content at the expense of  $C_6S_2H_3$ . This phenomenon is due to the formation of additional C–S–H resulting from the pozzolanic reaction of SF and its stability under hydrothermal treatment. TG curves and Table 2 depict quantitatively the effect of BFS and SF on the formation of  $C_6S_2H_3$  (Jaffeite). It is evident that the breaking of  $C_6S_2H_3$  (Jaffeite) formation is due to the presence of SF that lower the C/S ratio to more stable hydrated products and also to the formation of additional CSH via pozzolanic reaction.

The increase of mass loss at 0–200 °C and its decrease at 520–600 °C are tightly linked due to the stabilization effect of silica fume on C–S–H and pozzolanic activity leading to the formation of additional C–S–H and  $C_2ASH_8$  under hydrothermal curing, as it is demonstrated by the peak near 200 °C. The magnitude of this peak is found dependent on SF and BFS addition.

Moreover, three endothermic peaks are located at temperature range 650–700 and 750–800 and 850–1000 °C. Wongkeo et al. [23] have noticed the existence of the same endothermic peaks from thermal decomposition of ternary cement blends cured under different conditions. These thermal decompositions are characteristics for calcium carbonate originated from the carbonation of C–S–H and CH, such as waterite and calcite [17, 24, 25] that are the two polymorph modifications of calcium carbonate formed by carbonation. Apart from the two peaks characterizing the presence of calcium carbonate resulting from carbonation, the DTG curve of

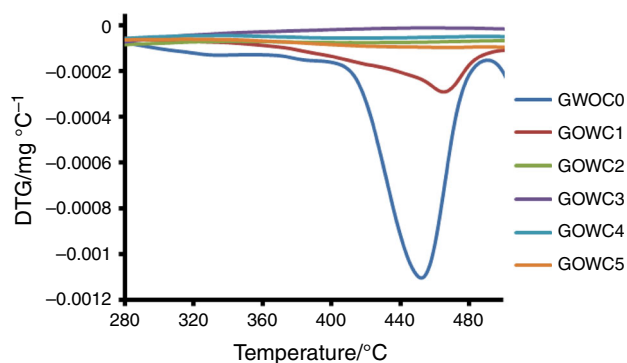


**Fig. 5** Influence of BFS and SF content on DTG characteristics of autoclaved samples in temperature interval 400–480 °C

GOWC5 with 50 mass% BFS shows an endothermic peak located at 900 °C that looks like the thermal decomposition of natural limestone. Indeed, limestone is generally used as slagging agent in the manufacture of pig iron to remove impurities and also it can be added to Portland cement (max 5 mass%). It is highly probable that the exothermic peak situated at 900 °C could be attributed to the decomposition of such limestone.

Temperature interval 700–1000 °C with exothermic peaks located at 800–900 °C was specially explored by considering the “equivalent” DSC curves. The exothermic heat flow denotes the crystallization of some products during thermal analysis measurement. Though the general ideas that the exothermic peaks at temperature 800–900 °C are due to the crystallization of mullite from glass phase in BFS, we found that the intensity of heat flow is a function of SF content and not that of BFS. The peak intensity of heat flow increases with increasing SF/GOWC (GOWC3-0.75, GOWC4-0.5, GOWC2-0.33, GOWC5-0.25, and GOWC1-0.125). DSC curve of GOWC0 does not represent any exothermic peak at this temperature range, as SF is missing.

Referring to the work carried out by Connan and co-workers on the formation of tobermorite and its influences upon the mechanical properties of autoclaved cement [14], exotherm above 800 °C on the DTG curve is due to the formation of wollastonite (CS) resulting from thermal transformation of 1.1 nm tobermorite [18, 23]. The increases of velocity of heat flow indicates that the proportion of tobermorite in the original reaction product had increased (Fig. 4). Considering these findings, it is evident that the crystallization of wollastonite results from the thermal transformation of tobermorite that the formation was supported by silica fume during the primary hydrothermal curing of the samples. SEM gives an evidence of fine crystalline phase of needle-like or honeycomb-like tobermorite phases (Fig. 5).

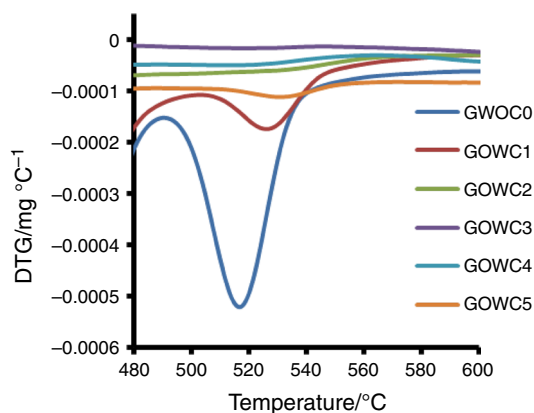


**Fig. 6** Influence of BFS and SF content on DTG characteristics of autoclaved samples in temperature interval 480–560 °C

### Mercury intrusion porosimetry measurements

Engineering properties of cement composites for oil well application such as strength, permeability and diffusivity (and thus durability), and shrinkage are associated with porosity and pore size distribution. The volume and size distributions of pores affect not only the mechanical strength of cement-based materials, but also its durability. The pore size distribution (PSD) of cement pastes cured under different hydrothermal regimes is depicted in Figs. 6 and 7. In order to determine the influences of the BFS and SF addition, two groups of curves are presented. The first group of curves serves to demonstrate the influence of increasing the addition of BFS and SF at constant ration on the pore structure, while the second one expresses the influence of increasing BFS/SF ratio at constant part of OPC. PSD of original GOWC is also presented in order to demonstrate the upgrade of pore structure. The effect of hydrothermal effect may be interpreted by the intensity and position of the peak, by the length and bimodal characteristic of PSD. The maximum concentration of pores in the G-Oil Well cement lies in the range  $10\text{--}10^3$  nm, and changes progressively to the size  $<10$  nm with increasing addition of BFS and SF. This behavior is attributed mainly to the presence of SF, as active micro-fillers. On the other hand, pozzolanic activities of both additives lead to the formation and stabilization of hydrated products as CSH gel or nano-size  $C_2ASH_8$  that fulfill the space between coarser particles. GOWC3 shows an incomplete PSD curve. It may be accepted that the maximum concentration of pore in autoclaved GWOC3 is localized in the nanopore area with R around 1 nm. In the mercury penetration method, all the pores in the gel cannot be measured owing to the difficulty of the high pressure technique and the minimum radius to be determined is 1.8 nm (by the

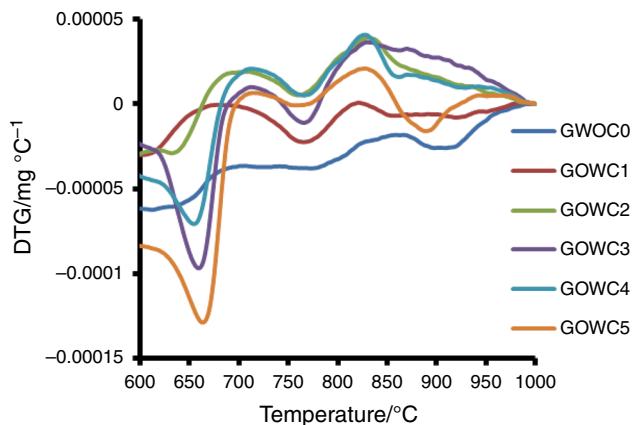


**Fig. 7** Influence of BFS and SF content on DTG characteristics of autoclaved samples in temperature interval 600–1000 °C

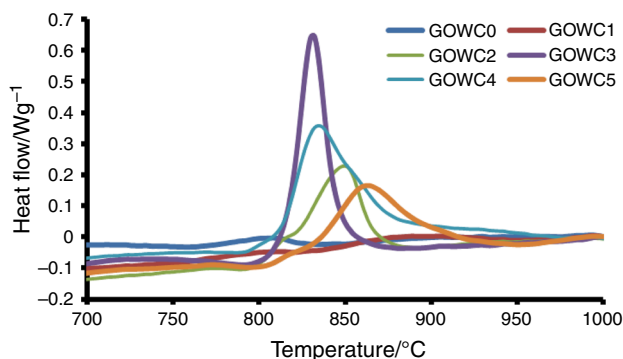


**Fig. 8** Influence of BFS and SF content on DSC heat flow in temperature interval 800–900 °C

pressure up to 400–440 MPa). From these results, it is evident that SF has greatly participated to the refinement of pore structure by forming and stabilizing CSH. The microstructure shows needle forms of hydrated products.

With increasing BFS/SF ratio, it can be remarked that the content of BFS contributes also to the refinement of pore structure. GOWC2 (20 % BFS + 20 % SF) and GOWC4 (40 % BFS + 20 % SF) PSD curves give an evidence that at the same content of SF, the amount of BFS consolidate the pore structure. This may be due to higher specific surface of BFS (Table 1) and also to the pozzolanic reaction occurred during autoclaving. In all cases, it is proved that the addition of admixture upgrade (Fig. 8).

Numerous studies report that the permeability of Oil well cement paste is of great importance, as it results from the measurable properties, such porosity and pore diameter. Greater permeability of set cement due to a greater porosity makes it sensitive to corrosive formation fluids which are an equally serious problem as losing the strength itself. Therefore, the permeability coefficient  $K$  becomes one of

**Table 4** Influence of BFS and SF addition on the permeability coefficient of autoclaved samples

Sample	Permeability coefficient/m s <sup>-1</sup>
GOWC0	$199 \times 10^{-15}$
GOWC1	$2.13 \times 10^{-15}$
GOWC2	$0.845 \times 10^{-15}$
GOWC3	$0.185 \times 10^{-15}$
GOWC4	$0.291 \times 10^{-15}$
GOWC5	$0.903 \times 10^{-15}$

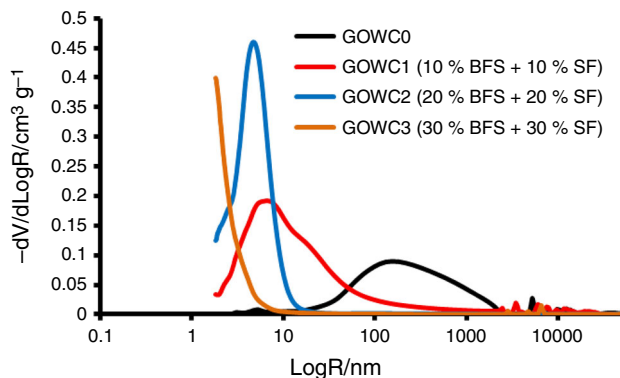


**Fig. 9** Influence of BFS and SF with constant ratio on PSD characteristics of autoclaved samples

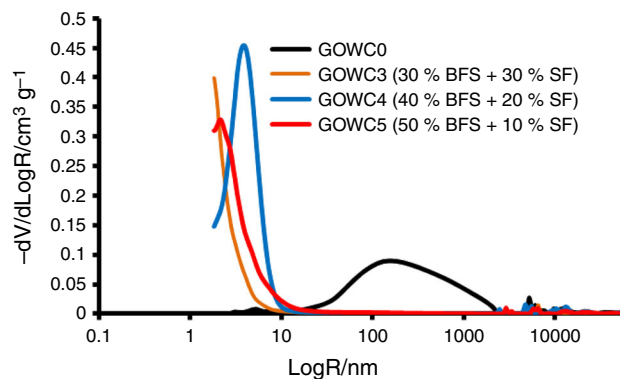


**Fig. 10** Influence of BFS and SF with increasing ratio on PSD characteristics of autoclaved samples

the essential characteristics used in the evaluation of cementitious materials for application in oil well. It is calculated by software Poremaster during porosimetric analysis according the following model:

$$K = \frac{\phi d_p^2}{32} \tag{1}$$

where  $\phi$  is the powder bed porosity and  $d_p$  the average pore diameter.

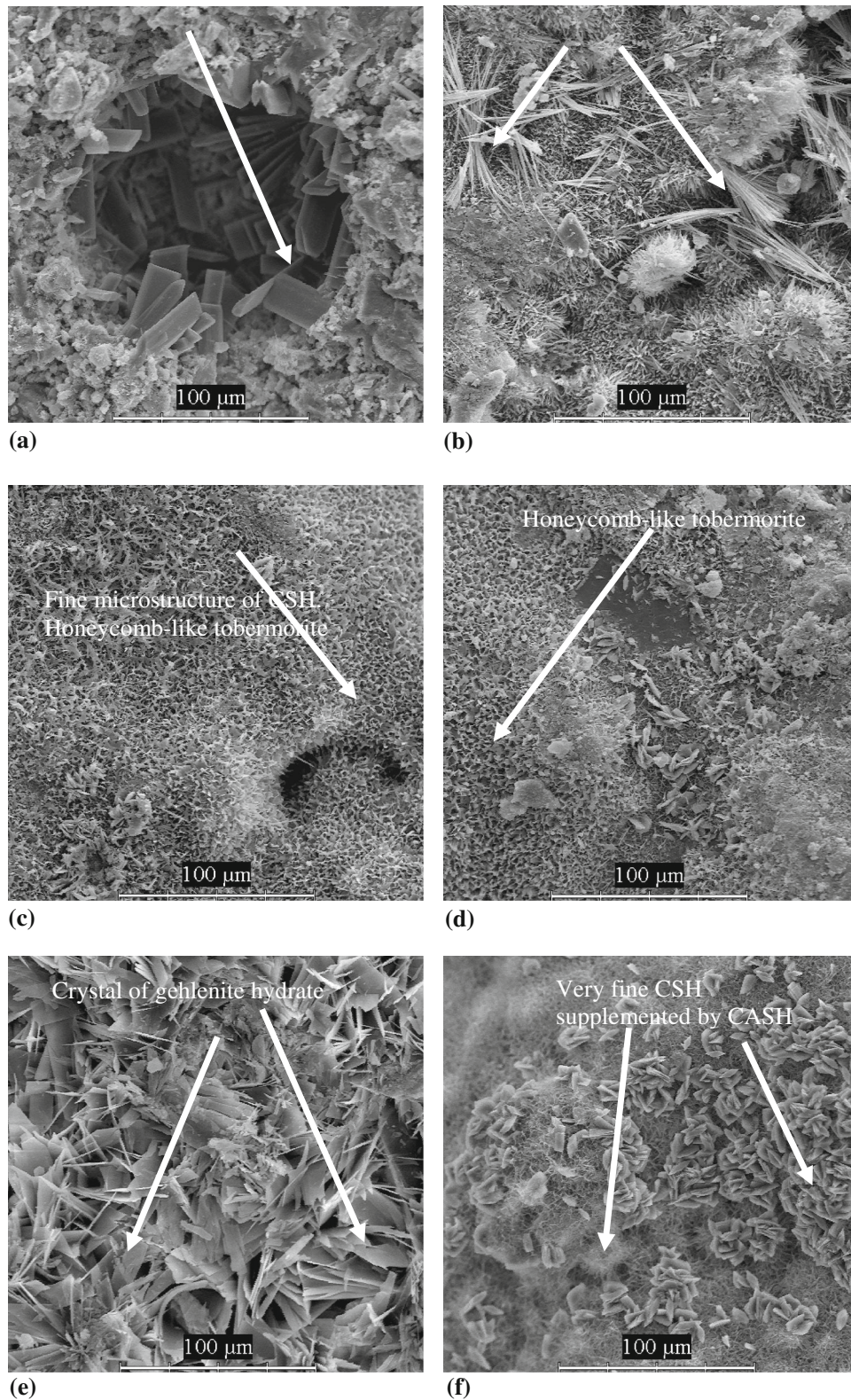


**Fig. 11** SEM micrographs of different GOWCs autoclaved at 200 °C and 1.2 MPa. **a** GOWC0, **b** GOWC1 (10 % BFS + 10 % SF), **c** GOWC2 (20 % BFS + 20 % SF), **d** GOWC3 (30 % BFS + 30 % SF), **e** GOWC4 (40 % BFS + 20 % SF), **f** GOWC5 (50 % BFS + 10 % SF)



As it can be seen in Table 4, the permeability coefficient has markedly decreased with increasing BFS and SF addition. The permeability coefficient of GOWC without addition is several times higher than that of blended ones. The significant decrease of permeability coefficient of GOWC due to the effect of BFS and SF addition proves again that the main property of GOWC has been improved and this makes them suitable for use in cementing oil or geothermal wells with higher temperatures and steam pressure (Figs. 9, 10).

#### Microstructure analysis

Other important changes occurred by addition of BFS and SF are demonstrated by SEM observations that show distinct size and morphology of hydrated products. For better comparison SEM micrographs with the same magnitude of 100  $\mu\text{m}$  are considered. SEM micrograph of G-Oil Well cement (GOWC0) cured at 200 °C/1.2 MPa as shown in Fig. 11a, reveal well-crystallized hydrated phases that have eventually caused the degradation of pore structure. These crystallized phases are mainly CH and  $\text{C}_6\text{S}_2\text{H}_3$  as it was proved by DTG analysis. SEM micrographs of blend GOWCs show distinct changes in the morphology and size of hydrated products. The needle forms found locally in autoclaved GOWC1 (Fig. 11b) paste is due to the pozzolanic reaction of SF that leads to the formation of calcium silicate hydrates with  $C/S = 1$  and then it hinders their transformation into larger crystal of  $\text{C}_6\text{S}_2\text{H}_3$ . Pore structure is consolidated (PSD curve) and the permeability coefficient lowered 200 times in comparison with that of GOWC without the addition of BFS and SF. Further increase in BFS and SF content has greatly modified the microstructure of autoclaved samples. One can remark the similarity between micrographs of GOWC2 and GOWC3 (Fig. 11c, d) due to the coupled effect of both additives. The refinement of microstructure from needle morphology to the fine network of honeycomb of hydrated products including pore with nano-size dimension is an evident demonstration of pore structure consolidation. The results of PSD curves have led to the same conclusion. Figure 11e, f shows fascinating SEM micrographs in which hydrated products present other morphology and size. Cured cement pastes are usually heterogeneous system including hydrated products with different particle and pore sizes. SEM micrograph of cured GOWC4 presents larger crystallized products, but with compact microstructure, while that of GOWC5 shows two distinct forms of products: very fine network of nano-size products supplemented by relative crystallized one.

#### Conclusions

Simultaneous addition of blast furnace slag (BFS) and silica fume (SF) has performed the mechanical and physical properties of G-Oil well cement cured under hydrothermal conditions of 200 °C and 1.2 MPa.

- Silica fume was responsible for the formation of additional C–S–H by pozzolanic reaction and also by reducing C/S ratio that hinders the transformation of C–S–H into  $\text{C}_6\text{S}_2\text{H}_3$ .
- Silica fume contributed to the refinement of pore structure as active micro-fillers occupying space between particles, reducing thus the permeability of hardened paste.
- Blast furnace with silica fume contributed to the formation of gehlenite hydrate  $\text{C}_2\text{ASH}_8$  that is stable under hydrothermal conditions.
- The transformation of CSH into  $\alpha\text{-C}_2\text{SH}$  and  $\text{C}_6\text{S}_2\text{H}_6$  was hindered. Also, the degree of replacement of G-Oil Well cement by combined silica fume and slag has gradually led to consumption of calcium hydroxide to form an additional CSH and calcium aluminosilicate hydrate, as it can be seen on DTG curve at 200 °C.

**Acknowledgements** This article has been produced with the financial assistance from VEGA No. 1/0064/12 and Project “Excellent young researchers at Brno University of Technology” under CZ.1.07/2.3.00/30.0039.

#### References

1. Zhang J, Weissinger EA, Peethamparan S, Scherer GW. Early hydration and setting of oil well. *Cem Concr Res.* 2010;40:1023–33.
2. Palou MT, Živica V, Ifka T, Boháč M, Zmrzlý M. Effect of hydrothermal curing on early hydration of G-Oilwell cement. *J Therm Anal Calorim.* 2013;113:1–7.
3. Nelson EB, Eilers LH, Kalousek GL. Formation and behavior of calcium silicate hydrates in geothermal environment. *Cem Concr Res.* 1981;3:371–81.
4. Le Saout G, Lécolier E, Rivereau A, Zanni H. Chemical structure of cement aged at normal and elevated temperatures and pressures part I. Class G oil well cement. *Cem Concr Res.* 2006;36:71–8.
5. Jupe AC, Wilkinson AP, Luke K, Funkhouser GP. Class H cement hydration at 180 °C and high pressure in the presence of added silica. *Cem Concr Res.* 2008;38:660–6.
6. Alunno VR, Chiochio G, Collepardi M. Influence of precuring on high pressure steam hydration of tricalcium silicate. *Cem Concr Res.* 1973;3:665–76.
7. Shaw S, Henderson CMB, Clark SM. Hydrothermal formation of hydrated calcium silicates: an in situ synchrotron study. *Am Miner.* 1998;62A:1337–78.
8. Ray A. Hydrothermally treated cement-based building materials. Past, present, and future. *Pure Appl Chem.* 2002;74:2131–5.

9. Palou MT, Bágel Ľ, Živica V, Kuliffayová M, Kozánková J. Influence of hydrothermal curing regimes on the hydration of fiber-reinforced cement composites. *J Therm Anal Calorim.* 2013;113:385–94. doi:[10.1007/s10973-013-2943-4](https://doi.org/10.1007/s10973-013-2943-4).
10. Midgley HG, Chopra SK. Hydrothermal reactions in the lime-rich part of the system  $\text{CaO-SiO}_2\text{-H}_2\text{O}$ . *Mag Concr Res.* 1960;12:19–24.
11. William CL, Gary JP. *Standard handbook of petroleum and natural gas engineering*, Second Edition, Linacre House, Jordan Hill, Oxford OX2 8DP, UK, 2005.
12. Luke K, Taylor HFW. Equilibria and non-equilibria in the formation of xonotlite and truscottite. *Cem Concr Res.* 1984;1984(5):657–62.
13. Land G, Stefan D. The influence of nano-silica on the hydration of ordinary Portland cement. *J Mater Sci.* 2012;47:1011–7.
14. Connan H, Klimesch D, Ray A, Thomas P. Thermal characterisation of autoclaved cement made with alumina-silica rich industrial waste. *J Therm Anal Calorim.* 2006;84:521–5.
15. Palou MT, Bágel Ľ, Živica V, Kuliffayová M, Ifka T. Hydration of high alumina cement–silica fume composite with addition of Portland cement or sodium polyphosphate under hydrothermal treatment. *J Therm Anal Calorim.* 2013;113:385–94. doi:[10.1007/s10973-013-3042-2](https://doi.org/10.1007/s10973-013-3042-2).
16. Chen W, Brouwers HJP. The hydration of slag, part 1: reaction models for alkali-activated slag. *J Mat Sci.* 2007;42:428–43. doi:[10.1007/s10853-006-0873-2](https://doi.org/10.1007/s10853-006-0873-2).
17. Ramachandran VS, Paroli RM, Beaudoin JJ, Delgado AH. *Thermal Analysis of Construction Materials, Handbook of thermal analysis of construction materials*. In: Ramachandra VS et al., editors. New York: Noyes Publications; 2002. p 118.
18. Richardson IG. The nature of C–S–H in hardened cements. *Cem Concr Res.* 1999;29:1131–47.
19. Kuliffayová M, Krajčí Ľ, Janotka I, Šmatko V. Thermal behaviour and characterization of cement composites with burnt kaolin sand. *J. Therm Anal Calorim.* 2012;108:425–32. doi:[10.1007/s10973-011-1964-0](https://doi.org/10.1007/s10973-011-1964-0).
20. Krajčí L, Janotka I, Jamnický P. Burnt kaolin sand as pozzolanic material for cement hydration. *Ceram Silik.* 2007;51:217–24.
21. Li C, Sun H, Li L. A review: The comparison between alkali-activated slag (Si + Ca) and metakaolin (Si + Al) cements. *Cem Concr Res.* 2010;40:1341–9.
22. Mostafa NY, El-Hemaly S, Al-Wakeel EI, El-Korashy SA, Brown PW. Characterization and evaluation of the pozzolanic activity of Egyptian industrial by-products I: Silica fume and dealuminated kaolin. *Cem Concr Res.* 2001;31:467–74.
23. Wongkeo W, Thongsanitgarn P, Chindaprasirt P, Chaipanich A. Thermogravimetry of ternary cement blends effect of different curing methods. *J Therm Anal Calorim.* 2013;113:1079–90. doi:[10.1007/s10973-013-3017-3](https://doi.org/10.1007/s10973-013-3017-3).
24. Janotka I, Krajčí Ľ, Ray A, Mojumdar SC. The hydration phase and pore structure formation in the blends of sulfoaluminate-belite cement with Portland cement. *Cem Concr Res.* 2003;33:489–97.
25. Drábik M, Gálíková L', Balkovic S, Slade RCT. Potential of Portland cements for MDF materials. *J Phys Chem Solids.* 2003;68:1057–61.